A Machine Learning Scheme for Estimating the Diameter of Reinforcing Bars Using Ground Penetrating Radar

Iraklis Giannakis, Antonios Giannopoulos, and Craig Warren

***Abstract*— Ground penetrating radar (GPR) is a well-established tool for detecting and locating reinforcing bars (rebars) in concrete structures. However, using GPR to quantify the diameter of rebars is a challenging problem that current processing approaches fail to tackle. To that extent, we have developed a novel machine learning framework that can estimate the diameter of the investigated rebar within the resolution range of the employed antenna. The suggested approach combines neural networks and a random forest regression and has been trained entirely using synthetic data. Although the training process relied only on numerical training sets, nonetheless, the suggested scheme is successfully evaluated with real data indicating the generalization capabilities of the resulting regression. The only required input of the proposed technique is a single A-scan, avoiding laborious measurement configurations and multisensor approaches. In addition, the results are provided in real time and making this method practical and commercially appealing.**

***Index Terms*— Concrete, diameter, ground penetrating radar (GPR), machine learning (ML), nondestructive technique (NDT), nondestructive testing, random forest (RF), rebar, regression.**

I. Introduction

GROUND penetrating radar (GPR) is a nondestructive technique (NDT) with a unique span of applications [1], ranging from glaciology [2], tree monitoring [3], and archeology [4] to landmine detection [5], forensic science [6], and planetary exploration [7]. GPR has been established as a mainstream NDT tool in civil engineering [8], and it has been successfully applied for building inspection and for detecting reinforcing bars (rebars) in concrete structures [9]. Various approaches using GPR have been suggested for locating and characterizing rebars [10], [11], and there are many commercial GPR systems that are custom-built for this purpose [12], [13]. Although GPR can reliably detect and locate rebars, assessing their quality and estimating their diameter are an ongoing area of research with, as of yet, no conclusive outcomes. Due to that, additional NDT methods (e.g., eddy current [11], electromagnetic induction [14], [15]) need to be applied in the field to complement GPR, raising the overall computational and operational costs, and adding complexity to the acquisition.

To address these issues, various signal processing approaches have been reported that try to establish a causal relationship between the diameter of the rebar and the received GPR signal [10], [16], [17]. However, these methods are based on simplified assumptions and they fail to provide a universal and reliable solution [11]. To tackle this, a detection algorithm based on full-waveform inversion (FWI) using shuffled complex evolution optimization has been suggested [18]. FWI is a holistic approach that keeps simplifications to a minimum and exploits all the available information embedded in the investigated signal. This gives rise to a robust detection tool that accurately manages to recover both the coordinates and the diameter of buried cylindrical targets [18]. Nonetheless, FWI is a time-consuming process, primarily due to the large computational resources necessary for the numerical evaluation of Maxwell's equations. Machine learning (ML) is gaining a renewed reputation within the GPR community due to the ability to provide real-time results for complex and computationally demanding problems [19]–[21]. In that context, a novel forward solver based on ML is described in [11]. A deep neural network (NN) is used in order to map the received waveform with respect to the depth of the rebar, the radius of the rebar, and the water fraction of the concrete [11]. The resulting forward solver is substantially faster than traditional electromagnetic numerical methods [11] and can accelerate FWI without compromising its accuracy [11]. In spite of that interpretation is still far from real time since the ML-based forward solver needs to be coupled with a global optimizer in order to avoid local minima that are present in the optimization space [11].

In this letter, an ML architecture is suggested in order to map the relationship between a single A-scan and the diameter of the underlying rebar without the need for FWI. The suggested scheme consists of two NNs and one random forest (RF) regression [22] that are coupled together to estimate the diameter of the rebar in real time. Similar to [11], the proposed ML framework is trained entirely using synthetic training sets. The generalization capabilities of this method are successfully tested using both numerical and real data.

Manuscript received October 14, 2019; revised January 21, 2020 and February 19, 2020; accepted February 26, 2020. Date of publication March 11, 2020; date of current version February 25, 2021. *(Corresponding author: Iraklis Giannakis.)*

Iraklis Giannakis is with the School of Computing and Engineering, University of West London, London W5 5RF, U.K. (e-mail: iraklis.giannakis@uwl.ac.uk).

Antonios Giannopoulos is with the School of Engineering, The University of Edinburgh, Edinburgh EH9 3FG, U.K. (e-mail: a.giannopoulos@ed.ac.uk).

Craig Warren is with the Department of Mechanical and Construction Engineering, Northumbria University, Newcastle NE1 8ST, U.K. (e-mail: craig.warren@northumbria.ac.uk).

Color versions of one or more of the figures in this letter are available online at https://ieeexplore.ieee.org.

Digital Object Identifier 10.1109/LGRS.2020.2977505

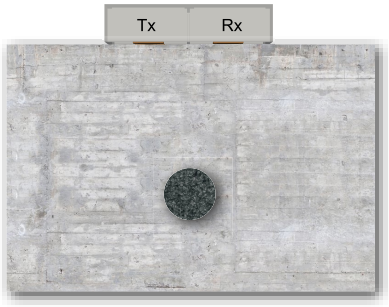

Fig. 1. Simulated scenario used for training the regression scheme. The antenna is the model equivalent of the GSSI 1.5-GHz antenna [13] and is placed directly above the rebar. The polarization of the antenna is parallel to the main axis of the rebar.

II. Methodology

A. Training Set

Supervised ML exploits information from labeled data in order to map the causal relationship (if there is one) between given inputs and their corresponding outputs [23]. To that extent, a well-labeled, coherent, and equally distributed training set is crucial during the training process and largely affects the overall performance of ML [23]. For estimating the diameter of rebars, obtaining such a training set from real data is time-consuming and not practical since it would require casting hundreds of concrete slabs with different water contents and different rebar characteristics. To overcome this, we employ a synthetic training set ensuring accurate labeling and avoiding unattainable experimental setups and undersized training sets.

The training data are generated using the ML-based forward solver described in [11]. The ML-based forward solver uses a deep NN architecture that accurately predicts the simulated A-scan based on the depth of the rebar, the diameter of the rebar, and the water fraction of the host concrete [11]. The ML solver is trained based on data generated using gprMax [24], [25]—an open-source electromagnetic simulator based on a second-order accurate finite-difference time-domain (FDTD) method [26]. The antenna used in the simulations is a model equivalent of a 1.5-GHz commercial GPR antenna made by Geophysical Survey Systems Inc. (GSSI) [13]. Consequently, the proposed regression scheme is tuned for the GSSI 1.5-GHz antenna, and therefore, using a different antenna system would require a new training set to be generated including a new model of that antenna. Fig. 1 illustrates the scenario under consideration during the training process. The GSSI 1.5-GHz antenna is placed directly above the rebar on the surface of the concrete. Using a single A-scan as input instead of a complete B-scan makes the process practical in the field and reduces the computational requirements necessary to generate the synthetic training data. This configuration (single A-scan) contains adequate information to fully recover the depth and the radius of the investigated rebar. The direct coupling provides information regarding the dielectric properties of the host medium while the amplitude and the arrival time of the reflected wave are associated with the depth and radius of the rebar. In particular, concrete slabs with higher water fractions act as a low pass filter which results in smoother cross-coupling. In addition, the reflection arrival time is associated with the water fraction of the concrete (derived from cross-coupling) and the depth of the target. Lastly, the amplitude of the reflected signal is related to the water fraction of the concrete (derived from the cross-coupling), the depth of the target (derived from the cross-coupling and the arrival time of the reflected wave), and the radius of the rebar. In conclusion, a combined sequential approach that utilizes all the available information embedded in an A-scan is capable of estimating the diameter of the rebar within the resolution of the employed antenna [11].

TABLE I
Extended Debye Properties of Concrete [28]

WC	ϵ_s	ϵ_∞	t_0 (ns)	σ $(\Omega^{-1}m^{-1})$
12 %	12.84	7.42	0.611	20.6×10^{-3}
9.3 %	11.19	7.2	0.73	23×10^{-3}
6.2 %	9.14	5.93	0.8	6.7×10^{-3}
5.5 %	8.63	6.023	1	5.15×10^{-3}
2.8 %	6.75	5.503	2.28	2.03×10^{-3}
0.2 %	4.814	4.507	0.82	6.06×10^{-4}

The rebar is modeled as a cylindrical perfect electrical conductor (PEC) with its main axis parallel to the polarization of the antenna. The dielectric properties of concrete are dispersive (similar to natural media [27]) and can be sufficiently approximated using an extended Debye model [11], [28]. The parameters of the Debye model—static permittivity, permittivity at infinite frequency, relaxation time, and conductivity—are expressed only with respect to the water content of the concrete [11], [28]. This is particularly attractive since it reduces the number of parameters necessary to fully describe the dielectric behavior of the host medium [11]. Table I illustrates the experimentally derived [28] properties of the extended Debye model with respect to the water fraction of the concrete. In a similar approach to [11], a spline interpolation is used in order to map the discrete properties shown in Table I in a continuous manner.

A training set consisting of 2000 samples has proven adequate for accurately resolving the investigated feature space. Increasing the number of samples beyond this value does not seem to affect the overall performance of the regression model. Each trace is simulated using a randomly selected set of the following three parameters.

1) Water content of concrete (*WC*).
2) Radius of the rebar (*R*).
3) Depth of the rebar (*D*).

Based on what is realistically expected in the field [11], the radius and the depth of the rebar vary from 2 to 25 mm and from 0 to 30 cm, respectively, while the water content ranges between 0.2% and 12% [28]. The proposed regression model is trained and validated within these ranges. Consequently, extrapolating this approach for cases outside the aforementioned bounds is not recommended.

B. Dimensionality Reduction

High-dimensional data give rise to a complex feature space that is difficult to be resolved without large training

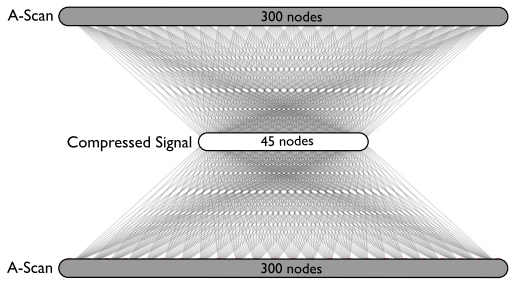

Fig. 2. Structure of the autoencoder used in this letter. The inputs and the outputs are the raw A-scans which consist of 300 points. The inner layer consists of 45 ReLU nodes that represent the compressed A-scan.

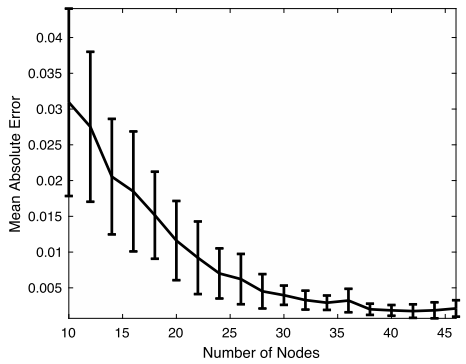

Fig. 3. Mean absolute error with respect to the number of nodes in the inner layer of the autoencoder (shown in Fig. 2). The error is calculated on normalized traces. The vertical bars correspond to the standard deviation.

sets and advanced learning algorithms [23], [29]. Therefore, dimensionality reduction is an essential aspect of ML, and various methodologies have been suggested for compressing the data prior to training [29]. One of the most mainstream and widely applied tools for compressing 1-D data is the autoencoder [30]. An autoencoder is an unsupervised NN that copies its inputs to the outputs. Autoencoders utilize the given training data $\mathbf{x} \in \mathbb{R}^n$ (n are the dimensions of the problem) and transform them to a revised representation $\mathbf{x}' \in \mathbb{R}^n$ that can be reproduced using a reduced number of dimensions (see Fig. 2).

Autoencoders consist of two parts: encoders and decoders. The encoder compresses the signal through

$$\mathbf{y} = \sigma(\mathbf{A}\mathbf{x} + b) \tag{1}$$

where $\mathbf{A} \in \mathbb{R}^{m \times n}$ is the weight matrix, b is the bias, σ is the activation function, $\mathbf{y} \in \mathbb{R}^m$ is the compressed signal, and m are the dimensions of the compressed signal ($m < n$). The compressed signal $\mathbf{y}$ is then decompressed in the decoder

$$\mathbf{x}' = \sigma(\mathbf{A}'\mathbf{y} + b') \tag{2}$$

where $\mathbf{A}' \in \mathbb{R}^{n \times m}$ and b' are, respectively, the weight matrix and the bias of the decoder. An autoencoder can be seen as an optimization process that tries to tune $\mathbf{A}$, $\mathbf{A}'$, b, and b' such as to minimize a given metric that describes the error between $\mathbf{x}$ and $\mathbf{x}'$.

Fig. 2 shows the autoencoder used for reducing the dimensions of the current training set. Each A-scan consists of 300 time-steps and is compressed to 45 nodes using a single hidden layer. The number of nodes in the hidden layer (m) is chosen so as to compress the signal effectively without compromising its resolution. The activation function of each node is a rectified linear unit (ReLU) [31]. Regarding the training process, an adaptive moment estimator (Adam) [32] is used that minimizes the mean squared error between $\mathbf{x}$ and $\mathbf{x}'$. A subset (80%) of the data described in Section II-A is utilized during the training process, while the rest are used for testing and validation purposes. Fig. 3 illustrates the error of the compression with respect to the number of nodes of the autoencoder. The error is calculated using data that were not used during the tuning of the autoencoder. It is apparent that the suggested compression scheme can effectively reduce the dimensions of the problem by a factor of 10 without compromising the information contained within the training set.

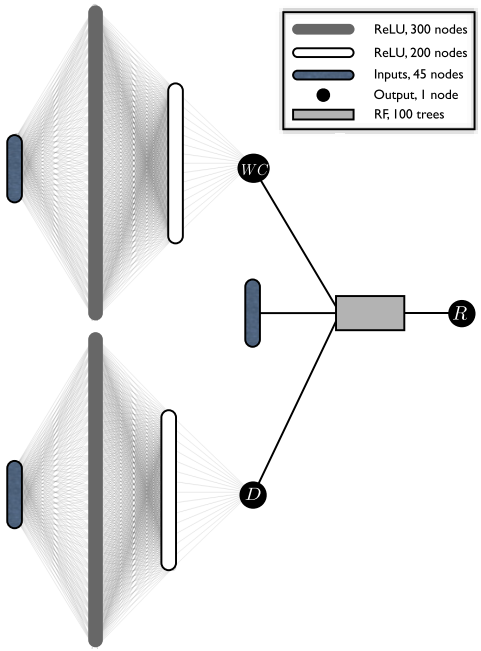

Fig. 4. Proposed detection scheme is a combination of two NNs regression models and one RF with 100 trees. The two NNs are trained independently to evaluate the water content and the depth of the rebar based on the compressed signal. Subsequently, the estimated water content and depth are combined with the compressed A-scan and used as inputs for RF. The output of the RF is the estimated radius of the rebar.

C. Regression Scheme

The regression scheme consists of two sequential steps. In the first step, two NNs are trained to predict the water fraction of the concrete WC and the depth D of the rebar based on a single compressed A-scan. Both NNs have two hidden layers with 300 and 200 nodes, respectively, as shown in Fig. 4. The activation functions of both layers are all ReLU apart from the last node which is linear. The synthetic data set is divided into three groups: 70% of the data are used for training, 10% are used for validation, and 20% are used for testing purposes. As with the autoencoder, Adam is employed in order to minimize the mean squared error between the actual and the estimated parameters.

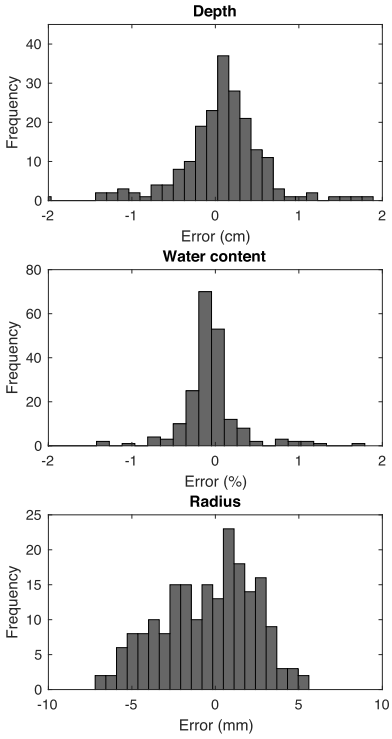

Fig. 5. Histograms of the errors between the actual and estimated parameters. The errors are calculated using unknown synthetic data, i.e., data that were not included in the training process.

In the second step, the estimated WC and D are coupled with the compressed A-scan $\mathbf{x}'$ to form the new input vector $\mathbf{q} = \langle WC,\ D,\ \mathbf{x}' \rangle$ (see Fig. 4). Subsequently, the vector $\mathbf{q}$ is used as input to a regression scheme based on RF with 100 trees. RF is an ensemble supervised learning scheme [22] with good performance in regression problems that often surpasses NN [33]. In this letter, RF has proven to perform better than NN for estimating the diameter of the rebar. Multiple NN configurations (different layers and nodes with different activation functions and various dropout layers) were tested using different optimizers and data batches. NNs become competitive only after applying bootstrap aggregating [34], however, RF still shows better generalization capabilities when applied to real measurements.

The split criterion of the trees in the RF tuned in this letter is the mean squared error, and the nodes are expanded until all the leaves are pure. The data set is divided into training (80%) and testing (20%) sets, and no bootstrap was used during the training. Fig. 5 illustrates the error between the actual (simulated) and the predicted (via our regression approach) parameters. The evaluation was done using unknown data that were not included in the training set. The depth D is accurately estimated with ± 2 cm maximum error and a standard deviation of less than ± 1 cm. The water content WC of the concrete is estimated with a maximum error at $\pm 2\%$ and a standard deviation of less than $\pm 1\%$. Subsequently, the estimated D and WC are coupled with the compressed A-scan $\mathbf{x}'$ in order to form the input vector $\mathbf{q}$. Based on $\mathbf{q}$, the radius of the rebar is estimated at ± 6 mm accuracy. As mentioned in [11], the discrepancies between the actual and predicted radii arise due to the inherent resolution of the employed GPR antenna,

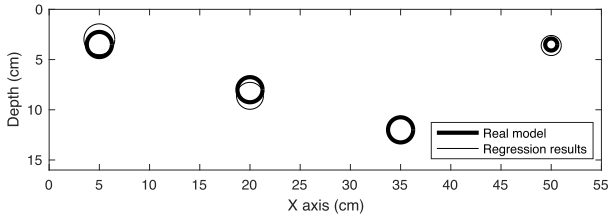

Fig. 6. Actual and the predicted rebar diameter and location using the proposed regression scheme. The inputs are real compressed A-scans collected with the antenna directly above the rebar on the surface of the (well-cured) concrete slab.

which is a function of its transmitted pulselength or center frequency (1.5 GHz). Consequently, the employed antenna has a minimum resolution (approximately 4 mm) that cannot be increased with typical signal processing approaches. In order to decrease the error, we need to increase the overall resolution by employing higher frequency antennas.

From the training data, it is apparent that the developed regression is suitable for single measurements on top of the rebar. Scenarios that deviate from this setup will likely result in errors and instabilities since they would lie out of the feature space that the ML-based scheme has been trained for. Consequently, the user will initially have to identify the apex of the hyperbola and subsequently apply the ML-scheme on that trace.

III. Laboratory Experiments

One of the novelties of the suggested regression scheme is that it is trained entirely using synthetic data. Although synthetic data are easy to gather (compared to real data), discrepancies between the real and the numerical A-scans will compromise ML and negatively affect the overall performance of the proposed approach. Accurate numerical frameworks should be employed in order for the ML to be effectively extrapolated to real measurements. Therefore, similar to [11], special care was taken to generate synthetic but nonetheless realistic and accurate training sets [13].

Four case studies are examined in order to evaluate the generalization capabilities of the suggested scheme and validate its performance using real data. The measurements were taken in the NDT laboratory at the School of Engineering, The University of Edinburgh. Four A-scans were collected using the GSSI 1.5-GHz antenna over four different rebars with different radii and varying depths. The polarization of the antenna was parallel with the main axis of the rebar in the same way that the synthetic data were generated. The raw A-scans were collected without any filtering (apart from the removal of static features) in order to match the modeled antenna [13] for which the ML was trained for.

Fig. 6 shows the actual and the predicted diameters as well as the locations of the rebars. The results are given in real time with minimum computational and operational requirements. It is apparent that both the depth and the radii of the rebars are accurately reconstructed, and the errors are within the expected ranges given when using the synthetic data. The estimated water content of the concrete varies from 10.6% to

11.8% which are in excellent agreement with the ones given in [11] using FWI. This indicates that the suggested regression scheme can be successfully extrapolated to real measurements providing real-time results from a single A-scan.

IV. Conclusion

A novel regression scheme has been described that can estimate the diameter of reinforcement bars in concrete using GPR. It requires a single A-scan as an input and provides the depth and diameter of the rebar as well as the water content of the concrete in real time. The regression consists of two NNs coupled with an RF. Both the NNs and the RF are trained independently using a coherent and well-labeled synthetic training data set. The raw data were effectively compressed using a shallow autoencoder in order to reduce the dimensionality of the problem and simplify training. The resulting approach has been successfully evaluated using both numerical and real data. This demonstrates that the proposed scheme can be reliably used with real measurements, despite the fact that it has been trained entirely using synthetic data. Therefore, data-driven processing tools can complement or potentially replace multisensor approaches, providing an accurate and real-time method for detecting and characterizing rebars in concrete structures.

References

[1] D. J. Daniels, *Ground Penetrating Radar*, 2nd ed. London, U.K.: Institution of Engineering and Technology, 2004.

[2] R. M. Williams, L. E. Ray, J. H. Lever, and A. M. Burzynski, "Crevasse detection in ice sheets using ground penetrating radar and machine learning," *IEEE J. Sel. Topics Appl. Earth Observat., Remote Sens.*, vol. 7, no. 12, pp. 4836–4848, Dec. 2014.

[3] I. Giannakis, F. Tosti, L. Lantini, and A. M. Alani, "Health monitoring of tree trunks using ground penetrating radar," *IEEE Trans. Geosci. Remote Sens.*, vol. 57, no. 10, pp. 8317–8326, Oct. 2019.

[4] L. B. Conyers, *Ground Penetrating Radar Archaeology*, Walnut Creek, CA, USA: AltaMira Press, 2004.

[5] I. Giannakis, A. Giannopoulos, and C. Warren, "A realistic FDTD numerical modeling framework of ground penetrating radar for landmine detection," *IEEE J. Sel. Topics Appl. Earth Observat., Remote Sens.*, vol. 9, no. 1, pp. 37–51, Jan. 2016.

[6] J. K. Pringle, J. R. Jervis, J. D. Hansen, G. M. Jones, N. J. Cassidy, and J. P. Cassella, "Geophysical monitoring of simulated clandestine graves using electrical and ground-penetrating radar methods: 0–3 years after burial," *J. Forensic Sci.*, vol. 57, no. 6, pp. 1467–1486, 2012.

[7] E. Pettinelli *et al.*, "Electromagnetic propagation of GPR signals in martian subsurface scenarios including material losses and scattering," *IEEE Trans. Geosci. Remote Sens.*, vol. 45, no. 5, pp. 1271–1281, May 2007.

[8] W. Wai-Lok Lai, X. Dérobert, and P. Annan, "A review of ground penetrating radar application in civil engineering: A 30-year journey from locating and testing to imaging and diagnosis," *NDT E Int.*, vol. 96, pp. 58–78, Jun. 2018.

[9] M. R. Shaw, S. G. Millard, T. C. K. Molyneaux, M. J. Taylor, and J. H. Bungey, "Location of steel reinforcement in concrete using ground penetrating radar and neural networks," *NDT E Int.*, vol. 38, no. 3, pp. 203–212, Apr. 2005.

[10] Z. Mechbal and A. Khamlichi, "Determination of concrete rebars characteristics by enhanced post-processing of GPR scan raw data," *NDT E Int.*, vol. 89, pp. 30–39, Jul. 2017.

[11] I. Giannakis, A. Giannopoulos, and C. Warren, "A machine learning-based fast-forward solver for ground penetrating radar with application to full-waveform inversion," *IEEE Trans. Geosci. Remote Sens.*, vol. 57, no. 7, pp. 4417–4426, Jul. 2019.

[12] C. Warren and A. Giannopoulos, "Creating finite-difference time-domain models of commercial ground-penetrating radar antennas using Taguchi's optimization method," *Geophysics*, vol. 76, no. 2, pp. G37–G47, Apr. 2011.

[13] I. Giannakis, A. Giannopoulos, and C. Warren, "Realistic FDTD GPR antenna models optimized using a novel linear/nonlinear full-waveform inversion," *IEEE Trans. Geosci. Remote Sens.*, vol. 57, no. 3, pp. 1768–1778, Mar. 2019.

[14] Ł. Drobiec, R. Jasiński, and W. Mazur, "Accuracy of eddy-current and radar methods used in reinforcement detection," *Materials*, vol. 12, no. 7, p. 1168, Apr. 2019.

[15] F. Zhou, Z. Chen, H. Liu, J. Cui, B. Spencer, and G. Fang, "Simultaneous estimation of rebar diameter and cover thickness by a GPR-EMI dual sensor," *Sensors*, vol. 18, no. 9, p. 2969, Sep. 2018.

[16] R. Zhan and H. Xie, "GPR measurement of the diameter of steel bars in concrete specimens based on the stationary wavelet transform," *Insight-Non-Destructive Test. Condition Monit.*, vol. 51, no. 3, pp. 151–155, 2009.

[17] A. Dolgiy, A. Dolgiy, and V. Zolotarev, "Optimal radius estimation for subsurface pipes detected by ground penetrating radar," in *Proc. 11th Int. Conf. Ground Penetrating Radar (GPR)*, Columbus, OH, USA, vol. 4, 2006, pp. 1–8.

[18] T. Liu, A. Klotzsche, M. Pondkule, H. Vereecken, J. van der Kruk, and Y. Su, "Estimation of subsurface cylindrical object properties from GPR full-waveform inversion," in *Proc. 9th Int. Workshop Adv. Ground Penetrating Radar (IWAGPR)*, Jun. 2017, pp. 1–4.

[19] K. Dinh, N. Gucunski, and T. H. Duong, "An algorithm for automatic localization and detection of rebars from GPR data of concrete bridge decks," *Autom. Construct.*, vol. 89, pp. 292–298, May 2018.

[20] J. B. Rodriguez, M. F. Pantoja, X. L. Travassos, D. G. G. Vieira, and R. R. Saldanha, "A prediction algorithm for data analysis in GPR-based surveys," *Neurocomputing*, vol. 168, pp. 464–474, Nov. 2015.

[21] I. Giannakis, A. Giannopoulos, and A. Yarovoy, "Model-based evaluation of signal-to-clutter ratio for landmine detection using ground-penetrating radar," *IEEE Trans. Geosci. Remote Sens.*, vol. 54, no. 6, pp. 3564–3573, Jun. 2016.

[22] G. Louppe, "Understanding random forests," Ph.D. dissertation, Dept. Appl. Sci., Elect. Eng. Comput. Sci., Univ. Liège, Liège, Belgium, 2014.

[23] M. C. Bishop, *Neural Networks for Pattern Recognition*, New York, NY, USA: Oxford Univ. Press, 1996.

[24] C. Warren, A. Giannopoulos, and I. Giannakis, "GprMax: Open source software to simulate electromagnetic wave propagation for ground penetrating radar," *Comput. Phys. Commun.*, vol. 209, pp. 163–170, Dec. 2016.

[25] C. Warren *et al.*, "A CUDA-based GPU engine for gprMax: Open source FDTD electromagnetic simulation software," *Comput. Phys. Commun.*, vol. 237, pp. 208–218, Apr. 2019.

[26] A. Taflove and S. C. Hagness, *Computational Electrodynamics: The Finite-Difference Time-Domain Method*, 2nd ed. Norwood, MA, USA: Artech House, 2000.

[27] H. Liu, B. Xing, H. Wang, J. Cui, and B. F. Spencer, "Simulation of ground penetrating radar on dispersive media by a finite element time domain algorithm," *J. Appl. Geophys.*, vol. 170, Nov. 2019, Art. no. 103821.

[28] T. Bourdi, J. E. Rhazi, F. Boone, and G. Ballivy, "Modelling dielectric-constant values of concrete: An aid to shielding effectiveness prediction and ground-penetrating radar wave technique interpretation," *J. Phys. D, Appl. Phys.*, vol. 45, no. 40, 2012, Art. no. 405401.

[29] P. Jindal and D. Kumar, "A review on dimensionality reduction techniques," *Int. J. Comput. Appl.*, vol. 173, no. 2, pp. 42–46, Sep. 2017.

[30] D. H. Ballard, "Modular learning in neural networks," in *Proc. AAAI*, 1987, pp. 279–284.

[31] Y. LeCun, Y. Bengio, and G. Hinton, "Deep learning," *Nature*, vol. 521, pp. 436–444, May 2015.

[32] D. P. Kingma and J. Ba, "Adam: A method for stochastic optimization," 2014, *arXiv:1412.6980*. [Online]. Available: http://arxiv.org/abs/1412.6980

[33] M. W. Ahmad, M. Mourshed, and Y. Rezgui, "Trees vs neurons: Comparison between random forest and ANN for high-resolution prediction of building energy consumption," *Energy Buildings*, vol. 147, pp. 77–89, Jul. 2017.

[34] B. Bakker and T. Heskes, "Clustering ensembles of neural network models," *Neural Netw.*, vol. 16, no. 2, pp. 261–269, Mar. 2003.